Journal of Power Sources 189 (2009) 1190–1198

Contents lists available at ScienceDirect

Journal of Power Sources

journal homepage: www.elsevier.com/locate/jpowsour

The partial state-of-charge cycle performance of lead-acid batteries

Taisuke Takeuchi[a,*], Ken Sawai[b], Yuichi Tsuboi[a], Masashi Shiota[a], Shinji Ishimoto[a], Nobumitsu Hirai[c], Shigeharu Osumi[a]

[a] GS Yuasa Power Supply Ltd., Kyoto,Japan
[b] GS Yuasa Corporation Ltd., Kyoto, Japan
[c] Division of Materials and Manufacturing Science, Graduate School of Engineering, Osaka University, Osaka, Japan

ARTICLE INFO

Article history:
Received 24 October 2008
Received in revised form 9 January 2009
Accepted 13 January 2009
Available online 20 January 2009

Keywords:
Lead-acid battery
Negative lug corrosion
Passivation
Stop and go vehicle

ABSTRACT

Negative plate lugs of flooded lead-acid battery were corroded during partial state-of-charge (PSoC) pattern cycle life tests simulated from stop and go vehicle driving.

Potential step was applied to Pb–Ca–Sn alloy electrode at various potential and time regimes, and the electrode surface was observed by in situ electrochemical atomic force microscope (EC-AFM) to investigate the corrosion mechanisms during the potential step cycles.

It was found out that the severe corrosion occurs when the oxidation of Pb to $PbSO_4$ and partial reduction of passive layer of $PbSO_4$ take turns many times. It was also found out that the periodic full charge, the optimization of the alloy composition, addition of the material that may make the reaction mechanism change to electrolyte were effective to suppress the corrosion rate.

1. Introduction

Car industry has been trying to reduce carbon dioxide as countermeasures against the global warming. Under this situation, recently, EV or HEV has been developed. Moreover, the stop and go vehicle that can improve the fuel efficiency with the easier system than EV or HEV has been developed, too.

When the flooded lead-acid battery is tested under the conventional SLI usage condition, the failure modes of the battery are mainly positive grid corrosion, growth or sulphation of the negative active material [1]. In the case of stop and go vehicle usage condition, however, the battery is usually used under the partial state-of-charge (PSoC) condition to charge effectively. It was also reported that the negative lugs were corroded severely [2].

Under specific potential conditions in the electrolyte, it has been found that Pb alloy can be easily corroded during potential step cycles around $Pb/PbSO_4$ equilibrium potential. Therefore, potential step cycle tests were performed at various anodic and cathodic potential of Pb alloy electrode to investigate the corrosion characteristics and countermeasures. The electrode surface during the potential step cycles was observed by in situ electrochemical atomic force microscope (EC-AFM) [3–7] to investigate the corrosion mechanisms. This observation technique is very useful for studying the electrode reactions in detail, because it can observe the electrode surface in sulfuric acid electrolyte directly. Various types of knowledge about the electrochemical reactions on the negative and positive electrodes of lead-acid batteries have been obtained through EC-AFM observation of the morphological changes on Pb and PbO_2 electrodes in sulfuric acid solution during oxidation and reduction.

Various alloy compositions and electrolyte additives were also evaluated as countermeasures against the negative lug corrosion on the battery side.

2. Experimental

2.1. Potential of negative plate during stop and go vehicle usage and conventional SLI usage

First, failure modes of the flooded lead-acid battery under the condition that was simulated form stop and go vehicle usage were examined. Fig. 1 shows the typical current profile of the stop and go vehicle usage. To compare the stop and go vehicle usage with the conventional SLI usage, the JIS light load endurance (LLE) test was examined. Fig. 2 shows the current profile of LLE test.

The 12 V/48 Ah (JIS-D23 type) flooded lead-acid battery was prepared.

The negative plate potential was measured in these tests with $Pb/PbSO_4$ (3.39 M H_2SO_4) reference electrode which was introduced by Sawai et al. [8]. The reference electrode was stable enough

* Corresponding author at: Technical Development Division, Industry Business Unit, GS Yuasa Power Supply Ltd., Nishinosho, Kisshoin, Minami-ku, Kyoto 601-8520, Japan. Tel.: +81 75 312 2123; fax: +81 75 316 3798.
E-mail address: taisuke.takeuchi@jp.gs-yuasa.com (T. Takeuchi).

0378-7753/$ – see front matter © 2009 Elsevier B.V. All rights reserved.
doi:10.1016/j.jpowsour.2009.01.022

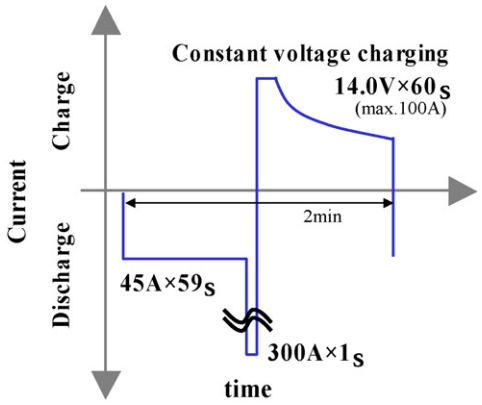

Fig. 1. The typical current profile simulated stop and go vehicle driving test.

to complete these tests. The potential of Pb/PbSO4 electrode is 355 mV more negative than that of the SHE [9].

2.2. Mechanism of negative lug corrosion

2.2.1. Potential step corrosion test

A three-electrode cell was assembled. Working electrode was Pb–0.06 mass% Ca–0.6 mass% Sn alloy rolled sheet. The electrode surface area was 24 cm^2 for both side. Counter electrode was Pb sheet with 120 cm^2 for both sides. Potential of working electrode was measured in these tests with $Pb/PbSO_4$ (3.39 M H_2SO_4) reference electrode.

Potential step corrosion tests were performed under conditions as follows.

Cycle regime was set to repeat each step at anodic potential for 30 s and cathodic potential for 30 s alternately. The cycle was repeated for 168 h (10,080 cycles).

(Test A) The test regime is shown in Fig. 3. Anodic potential was set at +40 mV, and cathodic potential was changed to investigate the potential region for severe corrosion, at 0 mV, −20 mV, −40 mV, −60 mV, −80 mV, −100 mV, −120 mV, −140 mV and −160 mV.

(Test B) The test regime is shown in Fig. 4. Cathodic potential was set at −80 mV and anodic potential was changed at +20 mV, +40 mV, +70 mV, and +100 mV.

(Test C) The test regime is shown in Fig. 5. More negative potential step at −160 mV was taken for 180 s with various intervals. The interval of the potential step at −160 mV was set at once per 20 min, 30 min, 1 h, and 2 h. They correspond to step at −160 mV every 17, 27, 57 and 117 cycles, respectively. These potential step cycles were also repeated for 168 h, and test cycles were changed due to each regime.

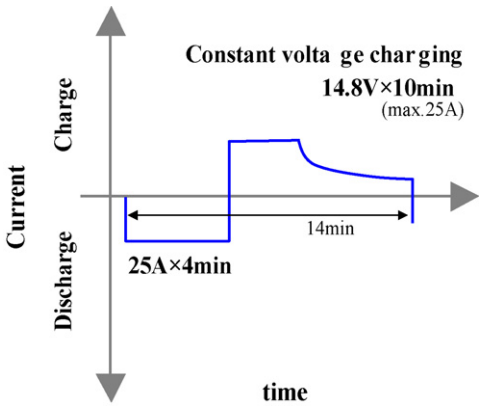

Fig. 2. The current profile of the JIS light load endurance (LLE) test.

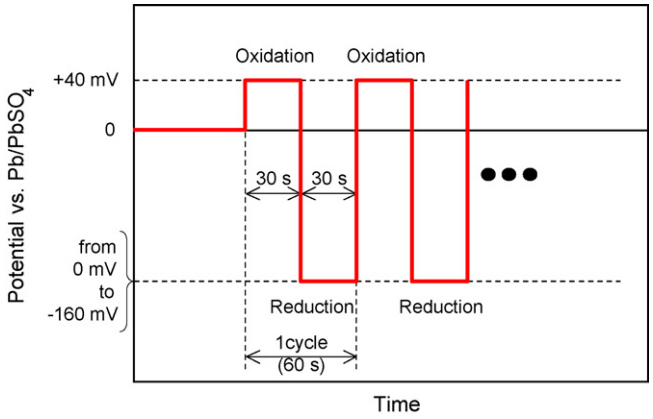

Fig. 3. Potential profile of working electrode in the potential step test A to measure mass loss by corrosion.

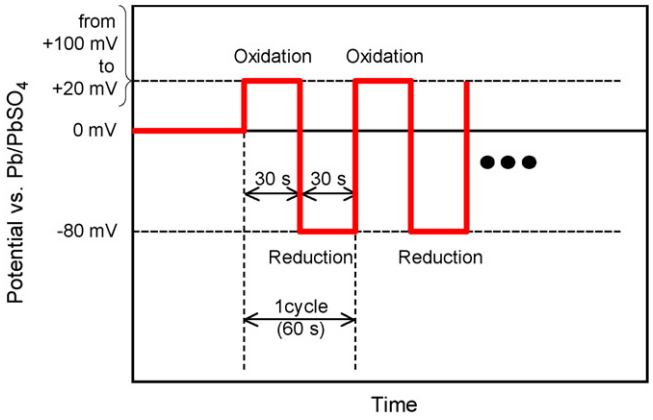

Fig. 4. Potential profile of working electrode in the potential step test B to measure mass loss by corrosion.

2.2.2. In situ – electrochemical atomic force microscope (EC-AFM) observation during potential step

Fig. 6 shows schematic illustration of the EC-AFM measurement. Working electrodes were Pb alloy rolled sheet. They were 100 mm in length, 20 mm in width. The alloy composition was Pb–0.06 mass% Ca–0.6 mass% Sn. Counter electrode was PbO_2 and reference electrode was Hg/Hg_2SO_4 (0.5 M H_2SO_4). The electrode potential will be converted to voltage vs. $Pb/PbSO_4$ (3.39 M H_2SO_4) in convenience.

Electrolyte was 3.39 M H_2SO_4 aqueous solution.

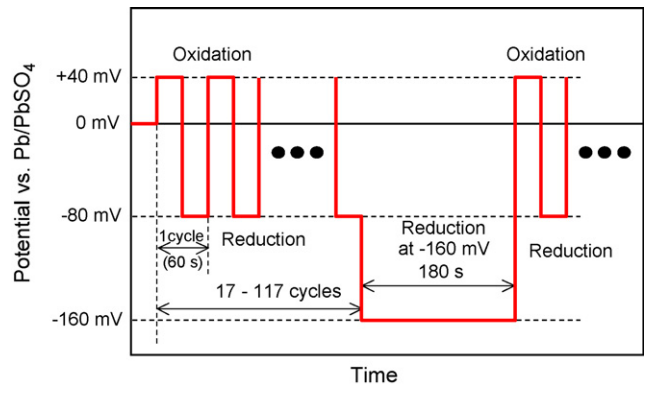

Fig. 5. Potential profile of working electrode in the potential step test C to measure mass loss by corrosion.

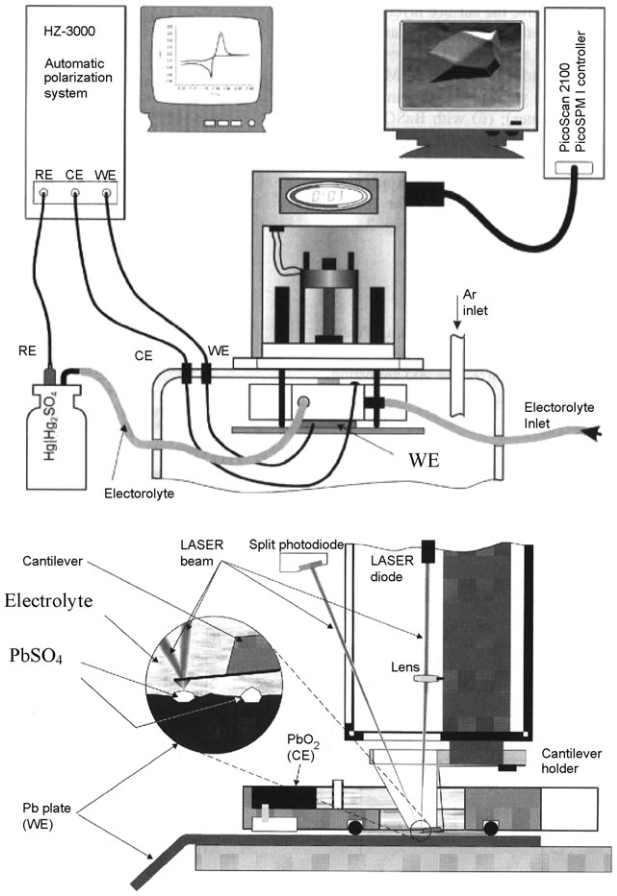

Fig. 6. Schematic illustration of the EC-AFM apparatus.

2.2.2.1. Electrode preparation. Surface of working electrode was polished with abrasive papers and then buffed with fine Al_2O_3 powder. Next, the electrode surface was polished chemically with a mixed solution of acetic acid and hydrogen peroxide, rinsed with distilled water, substituted with ethanol, and finally dried.

The working electrode was assembled into the EC-AFM cell, and then the cell was filled with 3.39 M sulfuric acid electrolyte. The electrode was reduced by two steps of potential, starting at −390 mV for 10 min followed by −190 mV for 10 min, to remove lead sulfate from the surface.

2.2.2.2. EC-AFM observation. Electrode surface morphology was observed by EC-AFM immediately after sample preparation. Fig. 7 shows time schedule for the EC-AFM observation and electrode potential step. Time for oxidation or reduction was 30 s, and the rest time for EC-AFM observation was 60 s. Cycle regime was varied to compare the surface morphology of the working electrode during cycling. The oxidation potential was set at +40 mV, and the reduction potential was set at −200 mV, −80 mV, and −20 mV. The same region of the electrode was observed in every cycle for each sample. The temperature was 25 °C through the whole experiment. The observed area for an AFM image was 10 μm × 10 μm, its mode was deflection mode, and its time per one image was 52 s.

2.3. Countermeasure against negative lug corrosion

Test cell was the same as described in Section 2.2.1. Potential step corrosion tests were performed under condition as follows.

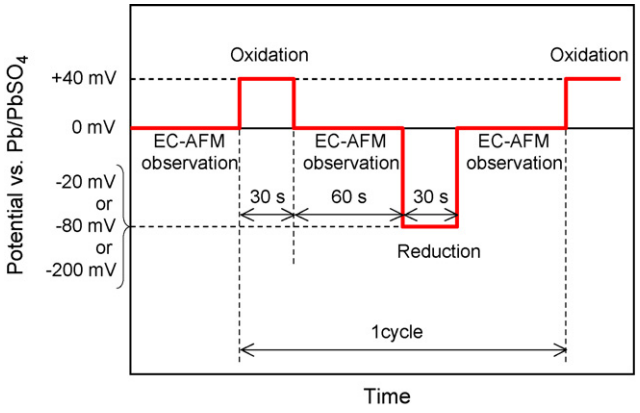

Fig. 7. Potential profile of working electrode to observe surface morphology by EC-AFM during potential step test.

Table 1
Composition of Pb–Sn alloy rolled sheet.

Sample no.	Content (mass%)
1	0
2	3
3	10
4	20
5	30
6	40
7	50

Table 2
Composition of Pb–Sb alloy rolled sheet.

Sample no.	Content (mass%)
1	0
2	0.9
3	4.0

Cycle regime was set to repeat each step at anodic potential for 30 s at +40 mV and cathodic potential for 30 s at −80 mV alternately. The cycle was repeated for 168 h (10,080 cycles).

In this study, various composition of the Pb–Sn alloy rolled sheet (Table 1) and the Pb–Sb alloy rolled sheet (Table 2) and electrolyte additives (Table 3) were examined.

EC-AFM observation was also performed to examine the mechanism. Table 4 shows the observation conditions. The other conditions were the same as described in Section 2.2.2.

3. Result and discussion

3.1. Potential of negative plate during stop and go vehicle usage and conventional SLI usage

When we carried out the cycle life test simulated from the stop and go vehicle usage, the battery was failed about 30,000 cycles. Then the battery was torn down to investigate the failure mode. We confirmed that the negative lugs were severely corroded. Especially the upper part of the negative lugs thin severely. Fig. 8

Table 3
Content of electrolyte addition.

Sample no.	Additive S	Content ($g\,l^{-1}$)
1	Control; non-addition	
2	H_3PO_4	5.0
3	$Sb_2(SO_4)_3$	0.5
4	$NiSO_4$	0.5
5	Lignin	0.2

Table 4
The conditions of EC-AFM observation.

Working electrode composition	Step condition	Potential vs. $Pb/PbSO_4$
Pb–50 mass% Sn	Potential step (Fig. 7)	
Pb–50 mass% Sn	Constant voltage for 1 min	−80 mV +50 mV +60 mV +70 mV +80 mV +90 mV +100 mV +110 mV
Pb–5 mass% Sb	Potential step (Fig. 7)	

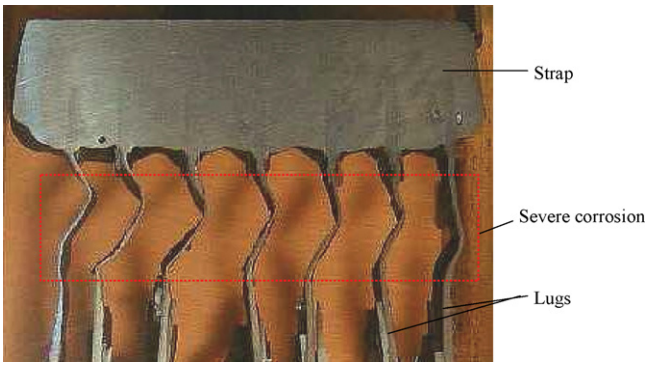

Fig. 8. Photograph of the cross-section of negative strap and lugs after the cycle life test simulated from stop and go vehicle driving.

shows the photograph of the cross-section of the negative strap and lugs after the cycle life test simulated from stop and go vehicle driving.

In the stop and go vehicle profile, the charge voltage is lower than that in the conventional SLI usage. Therefore, it is thought that batteries under the stop and go vehicle conditions gets a minimum amount of overcharge and are set under the PSOC condition. The negative plate potential during the stop and go vehicle driving test and LLE test are shown in Figs. 9 and 10, respectively. When the battery was discharged, each negative voltage were almost the same from +20 mV to +50 mV. On the other hand, when the battery was charged, the negative plate potential of stop and go driving test was from −50 mV to −110 mV and that of LLE test reached to −270 mV, they were quite different. From the above result, we deduced that the negative lug corrosion was more influenced by the potential during the charge where the reduction reaction takes place.

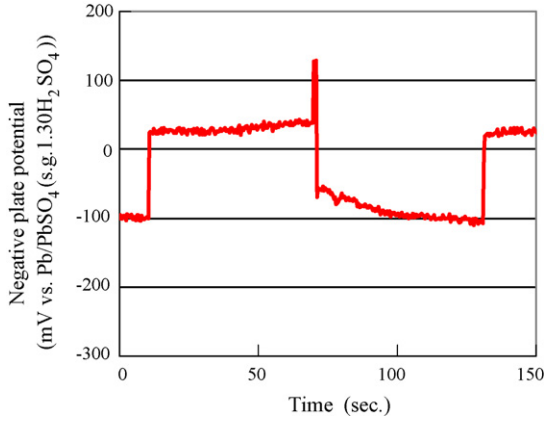

Fig. 9. The negative plate potential during the stop and go vehicle driving test.

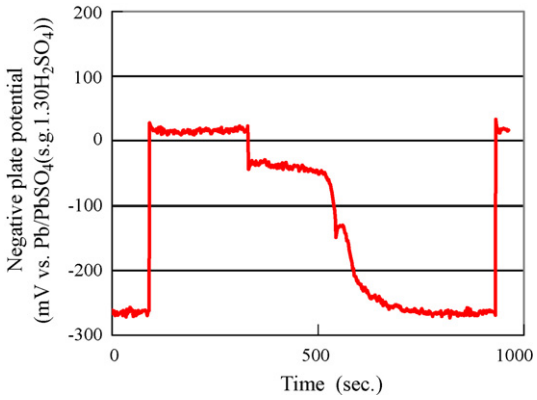

Fig. 10. The negative plate potential during the JIS light load endurance (LLE) test.

3.2. Mechanism of negative lug corrosion

3.2.1. Potential corrosion test

(Test A) Fig. 11 shows the mass loss of working electrode by corrosion during the potential step cycle. Working electrode was severely corroded at cathodic potential from −60 mV to −120 mV. Corrosion of working electrode was less when the cathodic potential of cycle was more positive than −60 mV or more negative than −120 mV. The maximum mass loss was 145 mg cm^{-2} during 168-h cycles at −80 mV cathodic potential. Corrosion layer of $PbSO_4$ cannot prevent the electrode surface from further oxidation during the specific potential step. Then the structure of the corrosion layer was observed. Fig. 12 shows photograph of the working electrode and corrosion layer in cross-section of the sample, after potential step cycles between +40 mV and −80 mV. The corrosion layer was made of $PbSO_4$. It shows that the corrosion layer was porous and uniform, unlike the grain boundary corrosion at the positive grid. It shows that the electrode repeated dissolution and precipitation and passive layer of dense $PbSO_4$ is not formed under these conditions. The corrosion layer was 0.4 mm thick measured from Fig. 12. The 145-mg cm^{-2} mass loss of the electrode is corresponding to 0.128 mm depth of corrosion on Pb alloy electrode surface. The volume becomes 3.1 times from 0.128 mm to 0.4 mm after the corrosion, because the density of $PbSO_4$ is lower than that of Pb metal, and the corrosion layer is porous.

(Test B) Fig. 13 shows the mass loss of working electrode by corrosion during the potential step cycle with various anodic potential. Mass loss of electrode increased steeply at +40 mV anodic poten-

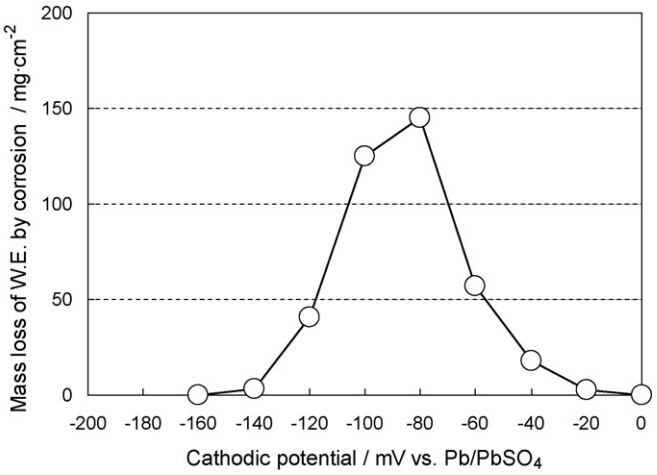

Fig. 11. Mass loss of working electrode during potential step corrosion test at various cathodic potential.

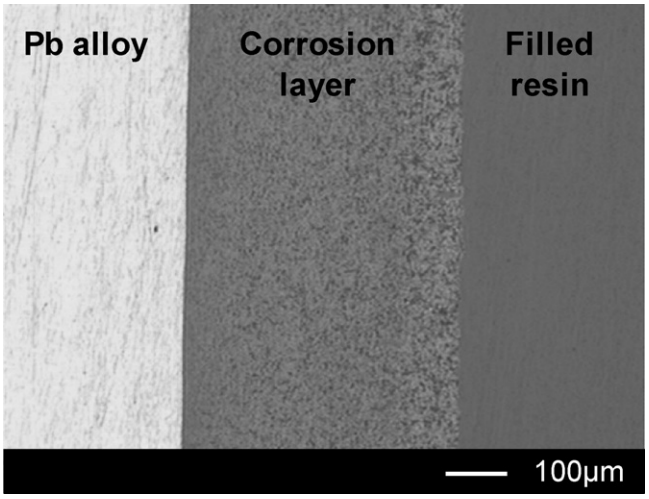

Fig. 12. The SEM photograph of cross-section of the working electrode after potential step test.

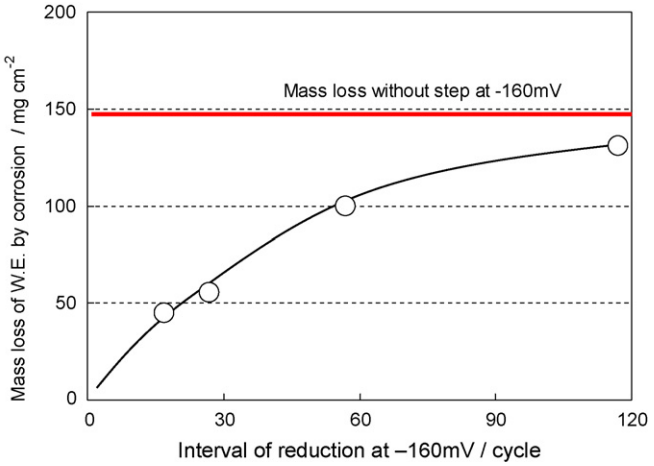

Fig. 14. Mass loss of working electrode during potential step corrosion test with cathodic polarization at −160 mV for 180 s at various intervals.

tial and remained at almost the same level when the anodic step potential was more positive than +40 mV. It shows that malfunction of passive layer against the corrosion is caused by the specific cathodic potential during cycling, and not by the anodic potential.

(Test C) Fig. 14 shows the mass loss of working electrode by corrosion during the potential step cycle with reduction step at −160 mV for 180 s with various intervals. The mass loss of electrode was decreased with more frequent reduction at −160 mV. It shows that corrosion layer formed during the oxidation–reduction cycles is reduced to metal Pb during cathodic polarization at −160 mV and corrosion does not proceed.

3.2.2. In situ AFM observation during potential step

Fig. 15 shows the EC-AFM images of electrode surface at initial state (Fig. 15(a)), after oxidation at +40 mV (Fig. 15(b)) and after reduction at −200 mV (Fig. 15(c)) of the same part of the working electrode surface at the first cycle.

At the initial state, the AFM image (Fig. 15(a)) shows the surface of Pb alloy. After the first oxidation, smooth particles of 5 μm or more covered the electrode surface (Fig. 15(b)). It shows that $PbSO_4$ particles were formed by oxidation on the surface. Then, after the first reduction, the particles disappeared (Fig. 15(c)). The surface image after the reduction is similar to that at the initial state (Fig. 15(a) and (c)). It shows that $PbSO_4$ particles on the surface were reduced to Pb. It was found out that $PbSO_4$ particles formed at anodic potential disappear at cathodic potential.

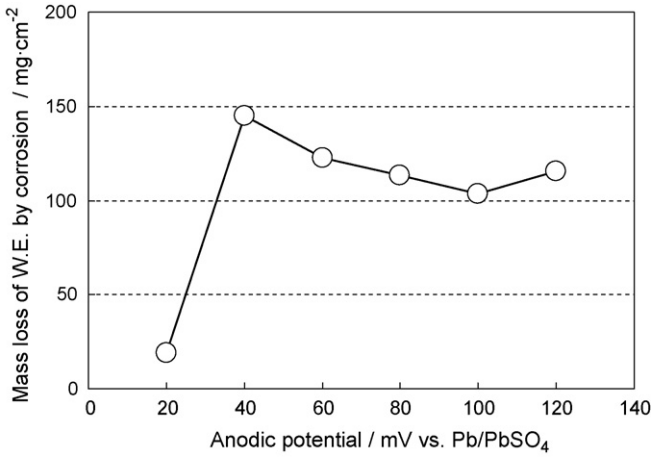

Fig. 13. Mass loss of working electrode during potential step corrosion test at various anodic potential.

Fig. 16 shows the EC-AFM images of electrode surface during potential step between +40 mV and −200 mV. The images were taken before the seventh cycle (Fig. 16(a)), and after oxidation at +40 mV (Fig. 16(b)) and after reduction at −200 mV (Fig. 16(c)) at the seventh cycle.

The surface image before the seventh cycle (Fig. 16(a)) is similar to that at the initial state (Fig. 15(a)). Particles, which were supposed to be $PbSO_4$, covered the electrode surface after oxidation at +40 mV (Fig. 16(b)), and they disappeared after reduction at −200 mV (Fig. 16(c)). Appearance of electrode surface seemed not to be changed before (Fig. 16(a)) and after the seventh cycle (Fig. 16(c)). It shows that $PbSO_4$ formed at anodic potential is reduced to metal Pb at −200 mV for 30 s in every cycles and corrosion does not proceed further.

Fig. 17 shows the EC-AFM images of electrode surface during potential step between +40 mV and −80 mV. The images were taken before the seventh cycle (Fig. 17(a)), after oxidation at +40 mV (Fig. 17(b)) and after reduction at −80 mV (Fig. 17(c)) at the seventh cycle.

The electrode surface was already partially covered with smooth particles of $PbSO_4$ (Fig. 17(a)). After oxidation (Fig. 17(b)), more $PbSO_4$ particles were formed at lower center and upper left corner of image, and the particle at left side grew larger. After the reduction (Fig. 17(c)), the particle at lower center disappeared. However, the particle at left side did not disappeared or seemed grown more, and the particles at upper left corner changed the shape and also did not disappeared. The electrode surface was covered more with $PbSO_4$ particles after (Fig. 17(c)) the seventh cycle than before (Fig. 17(a)). It was found out that $PbSO_4$ formed at anodic potential is not fully reduced to metal Pb at −80 mV for 30 s in every cycles and corrosion advances. Each $PbSO_4$ particle is not equally reduced, and some $PbSO_4$ particles are reduced to Pb and the other remained unreduced at −80 mV. $PbSO_4$ particles accumulate on the surface unevenly, and during repetition, porous corrosion layer is formed at the surface. Unreduced $PbSO_4$ particles could not be distinguished from reduced particles by their size or shape by the image (Fig. 17(b) and (c)). Other conditions like sulfuric acid concentration or local current density may affect reactivity.

Fig. 18 shows the EC-AFM images of electrode surface during potential step between +40 mV and −20 mV. The images were taken before the seventh cycle (Fig. 18(a)), after oxidation at +40 mV (Fig. 18(b)) and after reduction at −20 mV (Fig. 18(c)) at the seventh cycle.

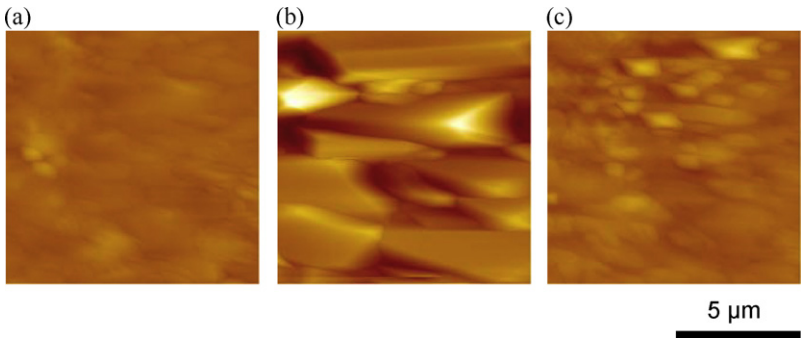

Fig. 15. The EC-AFM images of working electrode surface: (a) at the initial state; (b) after oxidation at +40 mV at the first cycle; (c) after reduction at −200 mV at the first cycle; of potential step test.

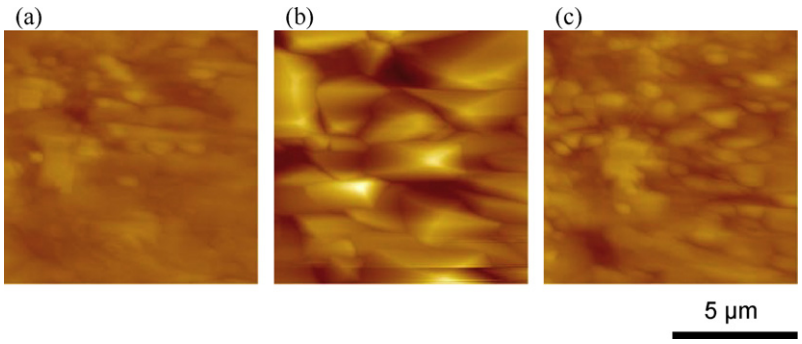

Fig. 16. The EC-AFM images of working electrode surface: (a) before oxidation at the seventh cycle; (b) after oxidation at +40 mV at the seventh cycle; (c) after reduction at −200 mV at the seventh cycle; of potential step test.

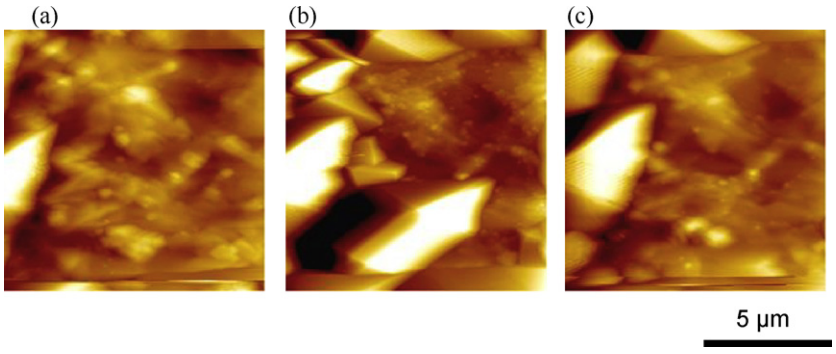

Fig. 17. The EC-AFM images of working electrode surface: (a) before oxidation at the seventh cycle; (b) after oxidation at +40 mV at the seventh cycle; (c) after reduction at −80 mV at the seventh cycle; of potential step test.

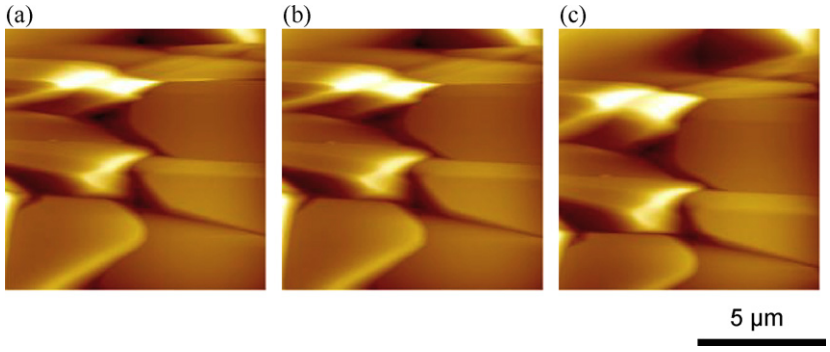

Fig. 18. The EC-AFM images of working electrode surface: (a) before oxidation at the seventh cycle; (b) after oxidation at +40 mV at the seventh cycle; (c) after reduction at −20 mV at the seventh cycle; of potential step test.

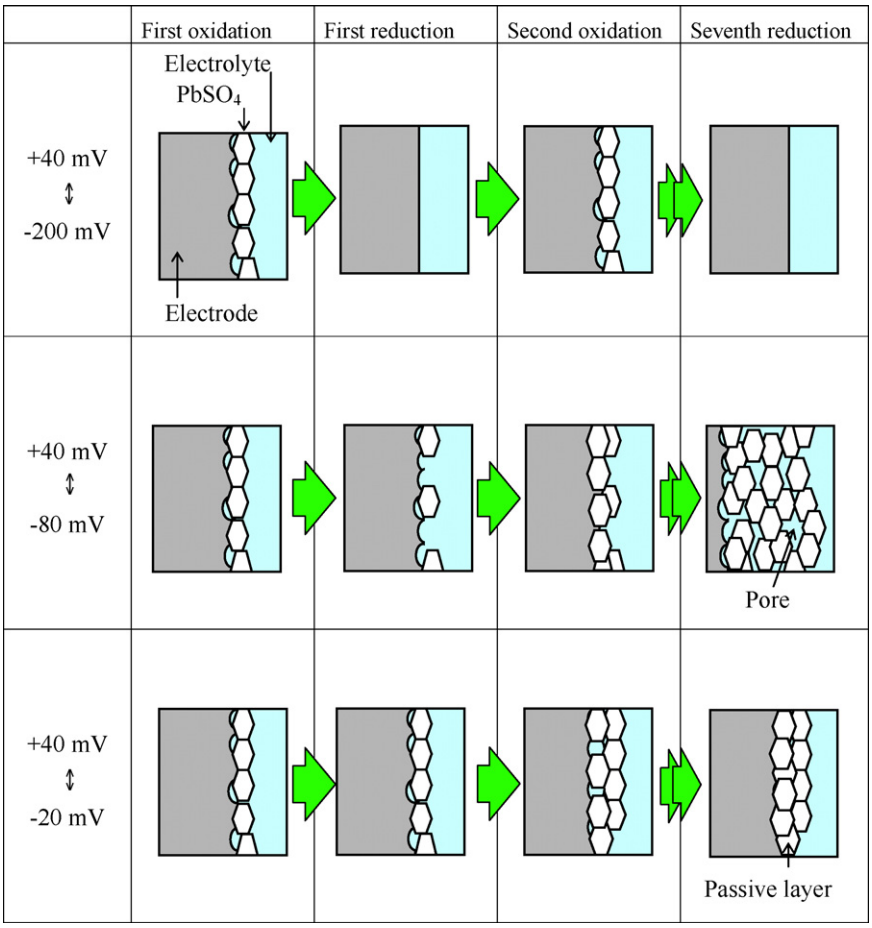

Fig. 19. Schematic diagram of corrosion mechanism during potential step cycles with various reduction potentials.

The electrode surface was already covered firmly with $PbSO_4$ particles (Fig. 18(a)), and little change was observed during the seventh cycle (Fig. 18(b) and (c)). The $PbSO_4$ particles seem to form passive layer and it cannot be reduced during step at −20 mV.

3.2.3. *Mechanism of corrosion during potential step*

Fig. 19 shows the schematic diagram of the corrosion mechanism during potential step cycles with various reduction potentials.

When the reduction potential is −200 mV, $PbSO_4$ formed at +40 mV is fully reduced at −200 mV for 30 s in every cycle and $PbSO_4$ does not accumulate.

The severe corrosion during the potential step cycle is caused by repetition of oxidation and reduction of Pb alloy. When the electrode potential is stepped between +40 mV and −80 mV, $PbSO_4$ formed at +40 mV is not fully reduced at −80 mV for 30 s and $PbSO_4$ accumulates gradually. Some of the $PbSO_4$ particles are reduced and the corrosion layer become porous, sulfuric acid can go into the deeper electrode surface, and the corrosion advances at the next +40 mV step. We think that the negative plate potential is under almost the same condition as this potential step test during the stop and go vehicle usage, so the negative lug corrosion proceeds.

When the reduction potential is −20 mV, $PbSO_4$ formed at +40 mV is not reduced at −20 mV for 30 s and $PbSO_4$ forms dense passive layer.

3.3. *Countermeasure against the negative lugs corrosion*

Effect of the content of Sn in the Pb–Sn alloy sheet for negative lug corrosion in the potential step is shown in Fig. 20. Mass loss is highly decreased by increasing Sn content more than 10 mass%. Fig. 21 shows the EC-AFM images of the electrode surface of Pb–50 mass% Sn alloy rolled sheet during the potential step test between +40 mV and −80 mV. $PbSO_4$ particles were hardly formed. Fig. 22 shows the EC-AFM images of the electrode surface of Pb–50 mass% Sn alloy rolled sheet held at constant voltage from −80 mV to +110 mV for 1 min. The electrode surface was not changed from −80 mV to +70 mV. Then, the changes of the electrode surface were seen at more positive than 80 mV. These changes seem the dissolution of Sn. Therefore, high Sn content alloy rolled sheet is difficult to corrode during the potential step test between +40 mV

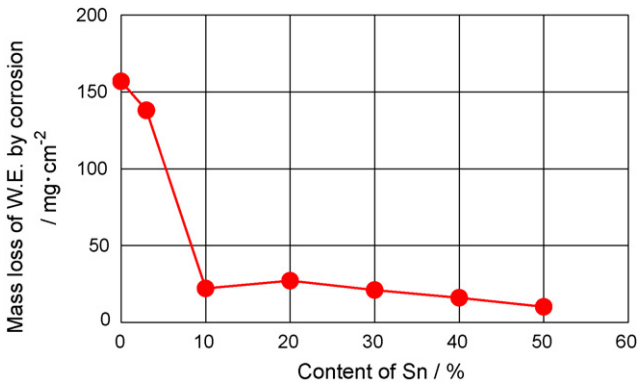

Fig. 20. Mass loss of working electrode during potential step corrosion test at various content of Sn in Pb–Sn alloy rolled sheet.

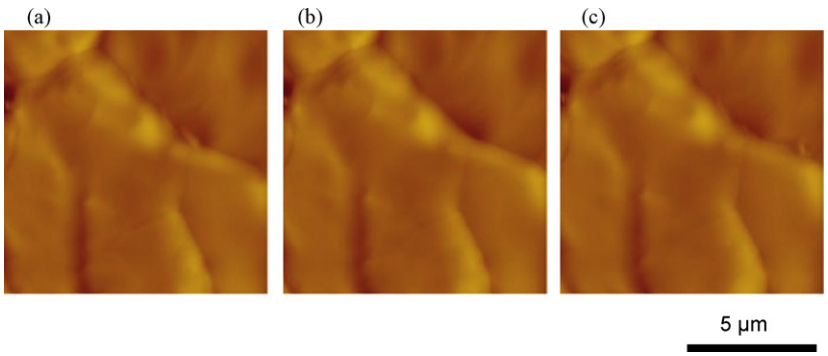

Fig. 21. The EC-AFM images of working electrode surface of Pb–50 mass% Sn alloy rolled sheet: (a) before oxidation at the seventh cycle; (b) after oxidation at +40 mV at the seventh cycle; (c) after reduction at −80 mV at the seventh cycle; of potential step test.

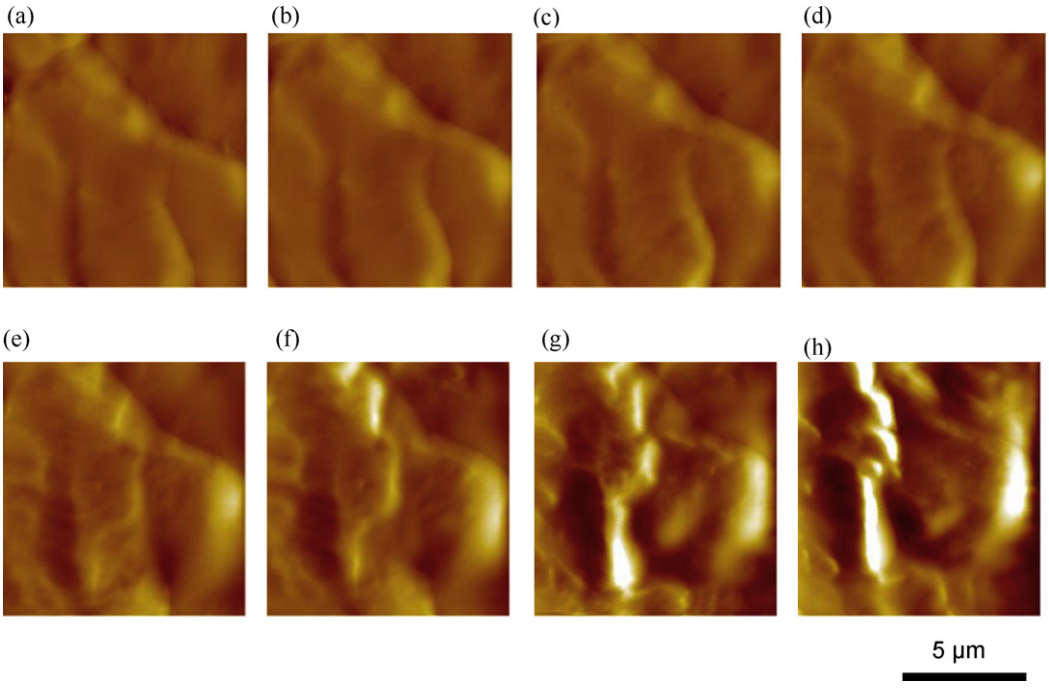

Fig. 22. The EC-AFM images of working electrode surface of Pb–50 mass% Sn alloy rolled sheet held at the constant voltages from −80 mV to +70 mV for 1 min: (a) −80 mV, (b) +50 mV, (c) +60 mV, (d) +70 mV, (e) +80 mV, (f) +90 mV, (g) +100 mV and (h) +110 mV.

and −80 mV. Effect of the content of Sb of the Pb–Sb alloy sheet for negative lugs corrosion in the potential step is shown in Fig. 23. The mass loss was decreased by increasing Sb content. The AFM images of the electrode surface of Pb–4 mass% Sb alloy rolled sheet during the potential step between +40 mV and −80 mV are shown in Fig. 24. The $PbSO_4$ particles that formed on the Pb–4 mass% Sb alloy rolled sheet were smaller than that in the control ones (Fig. 17). And the surface was not firmly covered by $PbSO_4$ particles. So, the corrosion rate became slow because the smaller $PbSO_4$ particles were easy to be charged, we think. So, the optimization of negative lug's composition is effective to suppress the corrosion rate on the battery side.

Fig. 25 shows the mass loss during the potential step when the various additives were added to electrolyte. The mass loss was highly reduced by addition of antimony sulfate, nickel sulfate and lignin. We also think the effect of lignin addition as blow. The $PbSO_4$ particles that were generated on the surface of the negative lugs by the negative lugs corrosion in the early potential step test form the passive layer on the surface of the negative lugs because lignin has the function of hindering the reduction of $PbSO_4$ particles [6,10].

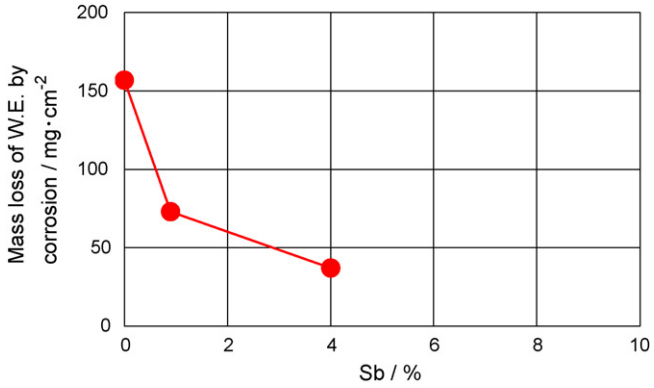

Fig. 23. Mass loss of working electrode during potential step corrosion test at various content of Sb in Pb–Sb alloy rolled sheet.

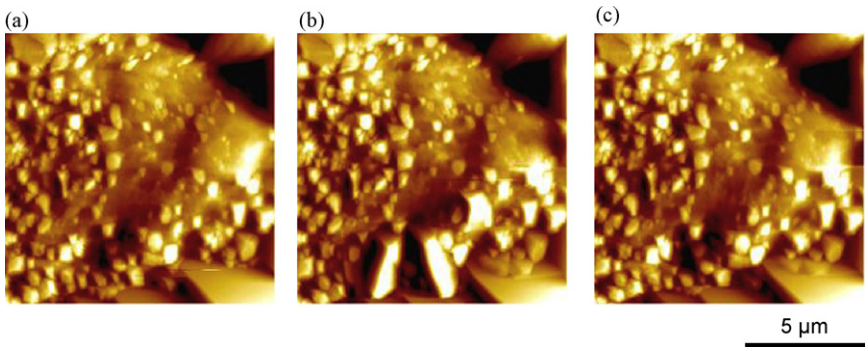

Fig. 24. The EC-AFM images of working electrode surface of Pb–4 mass% Sb alloy rolled sheet: (a) before oxidation at the seventh cycle; (b) after oxidation at +40 mV at the seventh cycle; (c) after reduction at −80 mV at the seventh cycle; of potential step test.

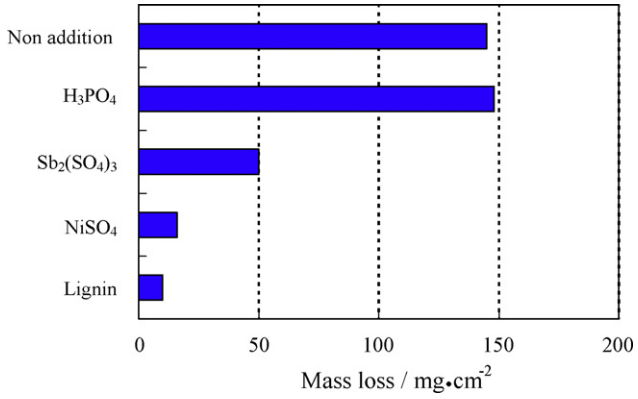

Fig. 25. Mass loss of working electrode during potential step corrosion test at various cathodic potential.

So, the corrosion does not proceed further. Therefore, the addition of these materials that make the reaction mechanism change is effective to suppress the corrosion rate on the battery side.

4. Conclusion

Negative lug corrosion of the flooded lead-acid battery was demonstrated during the potential step test simulated from the stop and go vehicle driving. Negative lugs were corroded by repetitions of charge and discharge that make negative lugs at a specific potential. Especially, potential during charge showed big influence on the corrosion. A mechanism of the negative lug corrosion of the flooded lead-acid battery under PSoC operation for the stop and go vehicle driving was proposed.

There is a possibility of suppressing the negative lug corrosion.

On the vehicle side:

- High charge voltage or periodic full charge.

On the battery side:

- The optimization of negative lug's alloy composition.
- Addition of the material that may make the reaction mechanism change to the electrolyte.

References

[1] H. Kohara, K. Konishi, A. Nanbu, N. Tsujino, S. Osumi, GS news technical report 46–2 (2) (1987) 11.
[2] T. Takada, D. Monma, J. Hurukawa, FB technical news 62 (2006) 16.
[3] Y. Yamaguchi, M. Shiota, Y. Nakayama, N. Hirai, S. Hara, J. Power Sources 85 (2000) 22.
[4] Y. Yamaguchi, M. Shiota, Y. Nakayama, N. Hirai, S. Hara, J. Power Sources 93 (2001) 104.
[5] Y. Yamaguchi, M. Shiota, M. Hosokawa, Y. Nakayama, N. Hirai, S. Hara, J. Power Sources 102 (2001) 155.
[6] N. Hirai, D. Tabayashi, M. Shiota, T. Tanaka, J. Power Sources 133 (2004) 32.
[7] H. Vermesan, N. Hirai, M. Shiota, T. Tanaka, J. Power Sources 133 (2004) 52.
[8] K. Sawai, Y. Tsuboi, M. Shiota, N. Hirai, S. Osumi, J. Power Sources 175 (2008) 604.
[9] The Electrochemical Society of Japan, Denkikagaku binran, (1985) 73.
[10] Central Laboratory for Electrochemical Power Source Bulgaria, S.E.A Tudor, Politecnico di Torino, Brite/Euram Project BE97-4085, Task 3, Improvements in negative plate performance, Final Report 1 January 1998 to 31 August 2001, Advanced Lead-Acid Battery Consortium, Research Triangle Park, NC, USA, 2001.